Journal of Structural Geology 89 (2016) 153–167

Contents lists available at ScienceDirect

Journal of Structural Geology

journal homepage: www.elsevier.com/locate/jsg

Hydrothermal frictional strengths of rock and mineral samples relevant to the creeping section of the San Andreas Fault

Diane E. Moore*, David A. Lockner, Stephen Hickman

U.S. Geological Survey, Earthquake Science Center, 345 Middlefield Road, Mail Stop 977, Menlo Park, CA 94025, USA

ARTICLE INFO

Article history:
Received 3 February 2016
Received in revised form
10 June 2016
Accepted 13 June 2016
Available online 16 June 2016

Keywords:
Frictional strengths
San Andreas Fault
SAFOD
Great Valley sequence
Franciscan complex
Saponite

ABSTRACT

We compare frictional strengths in the temperature range 25–250 °C of fault gouge from SAFOD (CDZ and SDZ) with quartzofeldspathic wall rocks typical of the central creeping section of the San Andreas Fault (Great Valley sequence and Franciscan Complex). The Great Valley and Franciscan samples have coefficients of friction, $\mu > 0.35$ at all experimental conditions. Strength is unchanged between 25° and 150 °C, but μ increases at higher temperatures, exceeding 0.50 at 250 °C. Both samples are velocity strengthening at room temperature but show velocity-weakening behavior beginning at 150 °C and stick-slip motion at 250 °C. These rocks, therefore, have the potential for unstable seismic slip at depth. The CDZ gouge, with a high saponite content, is weak ($\mu = 0.09–0.17$) and velocity strengthening in all experiments, and μ decreases at temperatures above 150 °C. Behavior of the SDZ is intermediate between the CDZ and wall rocks: $\mu < 0.2$ and does not vary with temperature. Although saponite is probably not stable at depths greater than ~3 km, substitution of the frictionally similar minerals talc and Mg-rich chlorite for saponite at higher temperatures could potentially extend the range of low strength and stable slip down to the base of the seismogenic zone.

Published by Elsevier Ltd.

1. Introduction

A major achievement of the San Andreas Fault Observatory at Depth (SAFOD), located along the creeping section of the San Andreas Fault (SAF), was the recovery of core containing the two strands of foliated gouge where creep was identified based on deformation of the well casing: the central deforming zone (CDZ) and the southwest deforming zone (SDZ) (Zoback et al., 2010, 2011) (Fig. 1). The creep rate at SAFOD is ~25 mm/yr (Titus et al., 2006), and the CDZ is considered to take up most of the slip, because of the significantly greater casing deformation associated with it. The CDZ and SDZ are fine-grained gouges, consisting largely of Mg-rich smectite clays produced by the low-temperature metasomatic alteration of serpentinite (e.g., Bradbury et al., 2011, 2015; Holdsworth et al., 2011; Moore and Rymer, 2012). They differ significantly in mineral assemblage from the adjoining quartzofeldspathic wall rocks of sedimentary origin, and the mineralogical differences are reflected in their room-temperature frictional properties (Lockner et al., 2011; Carpenter et al., 2012, 2015). The sedimentary rocks are relatively strong, with coefficients of friction, μ, that generally exceed 0.4. Strength changes abruptly across the boundaries of the wall rocks with the CDZ and SDZ, whose frictional strengths are largely in the range $\mu = 0.1–0.2$. The more slowly creeping SDZ is slightly stronger than the CDZ (Lockner et al., 2011). With very few exceptions, all of the core samples tested by Lockner et al. (2011) and Carpenter et al. (2012, 2015) were velocity strengthening at room temperature.

However, the applicability of the room-temperature data to deeper portions of the seismogenic zone is not known. To date, heated experiments on SAFOD core samples have been conducted exclusively on CDZ gouge and only at temperatures ≤120 °C (Coble et al., 2014; French et al., 2015). To address this question, we compared the frictional behavior of the CDZ and SDZ with quartzofeldspathic rock types characteristic of the creeping section at temperatures to 250 °C and over a range of velocities. We also report the results of the first heated experiments on a separate of the smectite clay saponite, a major component of the CDZ and SDZ, to determine its potential influence on gouge properties.

2. Samples tested in this study

Granitic and metamorphic rocks of the Salinian block form the

* Corresponding author.
E-mail addresses: dmoore@usgs.gov (D.E. Moore), dlockner@usgs.gov (D.A. Lockner), hickman@usgs.gov (S. Hickman).

http://dx.doi.org/10.1016/j.jsg.2016.06.005
0191-8141/Published by Elsevier Ltd.

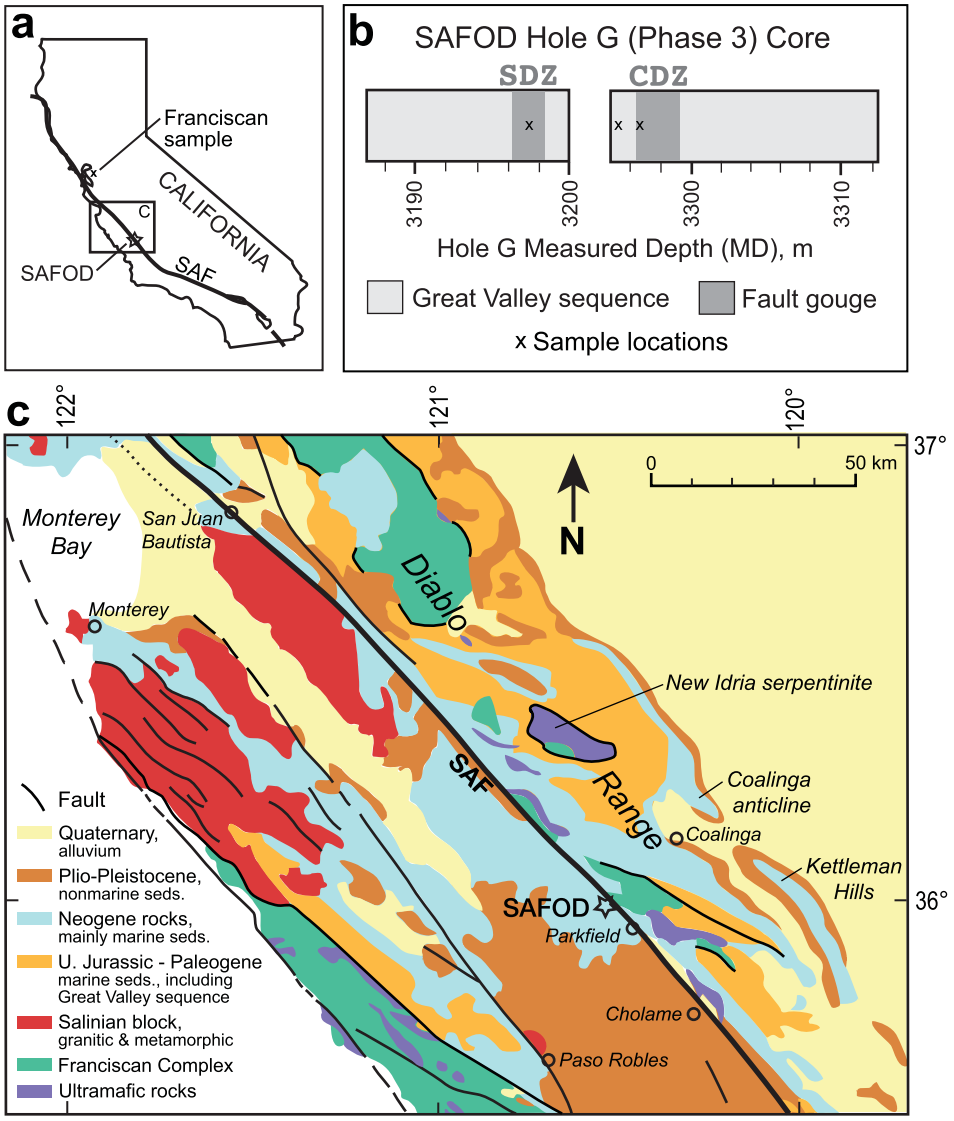

Fig. 1. Sample locations and regional geology of the creeping section of the San Andreas Fault (SAF). a) General sample locations. The Franciscan sample was collected in the San Francisco Bay area; the other three are from the SAFOD drillhole. The box outlines the area of the geologic map in c). b) Fault gouge and Great Valley sample positions in the SAFOD Hole G core. c) Simplified geologic and fault map of a portion of central California, modified from Jennings et al. (1977) with additional information from Page et al. (1998) and Titus et al. (2011). The SAFOD drillhole initiated in granitic rocks southwest of the SAF and terminated in the Great Valley sequence on the northeast side.

geologic basement southwest of the SAF creeping section, whereas the high P/T Franciscan metasedimentary rocks — largely meta-graywacke — of subduction zone origin comprise the basement of the Diablo Range on the northeast side (Fig. 1c). Another major rock unit in the Diablo Range is the sedimentary Great Valley sequence, which was deposited in a forearc basin on oceanic basement of the Coast Range ophiolite (e.g., Bailey et al., 1964; Ernst, 1965, 1970, 2011; Hamilton, 1969). The SAFOD drillhole terminated in rocks of the Great Valley sequence (Zoback et al., 2010, 2011), and the serpentinite in the CDZ and SDZ is derived from the Coast Range ophiolite (Moore and Rymer, 2012). Although Franciscan meta-sedimentary rocks were not encountered in the drillhole, they outcrop along the fault at SAFOD (Fig. 1c). The Franciscan Complex is a major component of the bedrock geology of the San Andreas system in central and northern California. One sample each representative of the Franciscan Complex and Great Valley sequence were selected for comparison with the CDZ and SDZ (Table 1). The samples chosen were ones with relatively high phyllosilicate contents and correspondingly lower frictional strengths, to minimize the contrast with the very weak, clay-rich gouge of the creeping traces.

The spot core at the bottom of the main SAFOD drillhole was identified as belonging to the Great Valley sequence, based on its fossil assemblages (Zoback et al., 2010, 2011). Although not directly determined to be Great Valley rocks, the sedimentary rocks in the section of core containing the CDZ (Hole G, Runs 4–6) are also fossiliferous and their clast populations and mineral assemblages closely resemble the Great Valley sequence rocks in the main hole (e.g., Holdsworth et al., 2011). The selected sample comes from the banded siltstone unit (Bradbury et al., 2011) on the SW side of the CDZ, at 3295.25 m measured depth (MD) (Fig. 1b). Its phyllosilicate mineral assemblage includes chlorite, illite and mixed-layer clays, and variably chloritized biotite (Figs. 2a and 3a). Intact pieces of siltstone from this same depth have been used for permeability measurements (Morrow et al., 2014) and petrographic studies (Moore, 2014). Its room-temperature frictional strength is in the middle of the range for the sedimentary rocks on either side of the CDZ (Lockner et al., 2011).

Table 1
Experiments conducted.

Sample	T (°C)	Jacket	Axial vel. range (μm/s)	Examination[a]
Great Valley	25	Pb	0.001–1.0	ThS
	100	Pb	0.001–1.0	
	150	Pb	0.001–1.0	ThS
	200	Pb	0.001–1.0	ThS
	250	Cu	0.001–10.0	SEM, XRD
Franciscan	25	Pb	0.001–1.0	
	100	Pb	0.001–1.0	ThS
	150	Pb	0.001–1.0	ThS
	200	Pb	0.001–1.0	ThS
	250	Cu	0.001–10.0	SEM, XRD
CDZ	25	Pb	0.001–1.0	ThS
	100	Pb	0.001–1.0	XRD, ThS
	150	Pb	0.001–1.0	XRD
	200	Pb	0.001–1.0	ThS
	250	Cu	0.001–10.0	SEM, XRD
SDZ	25	Pb	0.001–1.0	
	100	Pb	0.001–1.0	XRD
	150	Pb	0.001–1.0	XRD
	200	Pb	0.001–1.0	XRD, ThS
	250	Cu	0.001–10.0	
Saponite	25	Pb	0.001–1.0	
	100	Pb	0.001–1.0	XRD
	200	Pb	0.001–1.0	XRD

[a] ThS, thin section; SEM, scanning electron microscope; XRD, X-ray diffraction.

temperature frictional strength experiments. The prepared gouge had been ground and sieved to <90 μm grain size.

The CDZ sample, from 3296.66 m MD in Hole G, is located ~0.06 m from the contact of the CDZ with the banded siltstone (Fig. 1b). The SDZ sample comes from the center of the SDZ, at 3197.23 m MD (Fig. 1b). Both the CDZ and SDZ are Mg-clay-rich foliated gouges (Fig. 2c and d), the matrix clays consisting principally of saponite in the CDZ and saponite + corrensite in the SDZ (Fig. 3c and d; see also Moore, 2014). Sedimentary and serpentinite porphyroclasts are more abundant in the SDZ than the CDZ. The SAFOD core samples were ground and sieved to <150 μm grain diameter (Lockner et al., 2011).

At this time, only qualitative estimates of total phyllosilicate contents of the samples can be provided. Attempts to analyze the SAFOD XRD data with standard software programs did not yield proper mineral identifications or proportions, because many of the peaks from different minerals coincide (Fig. 3). Mineral identifications in this study were verified by petrographic and scanning microscope and electron microprobe analyses. The Great Valley and Franciscan (Morrow et al., 2010) samples are estimated to contain ~35–45% phyllosilicates. The saponite content of the CDZ was estimated at ~65% (Lockner et al., 2011), with serpentine adding an additional 15–20%. The combined phyllosilicate contents of the

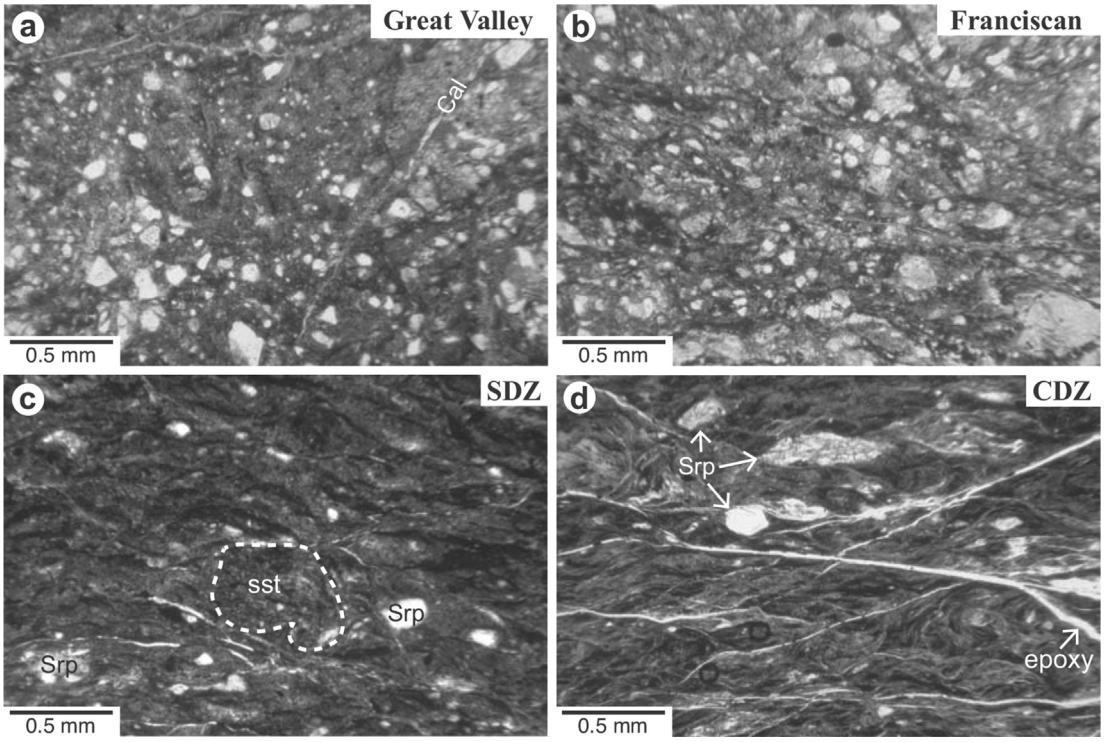

Fig. 2. Photomicrographs of rock samples (plane-polarized light). a) SAFOD Hole G core sample representative of the Great Valley sequence in the damage zone, 3295.23 m MD, cut by a calcite (Cal) vein; b) matrix of Franciscan Central belt mélange, surface outcrop from El Cerrito, San Francisco Bay area, CA (Morrow et al., 2010); SAFOD Hole G core from the c) SDZ and d) CDZ. Lockner et al. (2011) used fragmented SDZ and CDZ core materials for laboratory experiments, and two of their samples were tested in this study. The photomicrographs are of nearby intact core samples of closely comparable mineralogy and texture to the tested SDZ and CDZ samples, at 3197.0 m MD (SDZ) and 3296.6 m MD (CDZ), respectively. The gouges commonly separate along slickensided surfaces (curved, epoxy-filled white lines). The two creeping traces contain porphyroclasts of serpentinite (Srp) and crustal rocks; a siltstone porphyroclast in c) is outlined by a dashed white line.

The Franciscan sample represents the matrix of Central belt mélange, and it contains chlorite and phengitic white mica in addition to quartz and albite (Figs. 2b and 3b). It comes from an outcrop located near the Hayward Fault in the San Francisco Bay area (Fig. 1a), and it was the weakest of three Franciscan metasedimentary rock types that Morrow et al. (2010) tested in room-

SDZ, largely saponite + corrensite + serpentine, are somewhat lower than for the CDZ at ~65–70%.

To date only a single, room-temperature friction experiment on saponite has been reported (Lockner et al., 2011). A pure saponite separate could not be obtained from the CDZ or SDZ gouges, because of the presence of other phyllosilicate minerals, notably

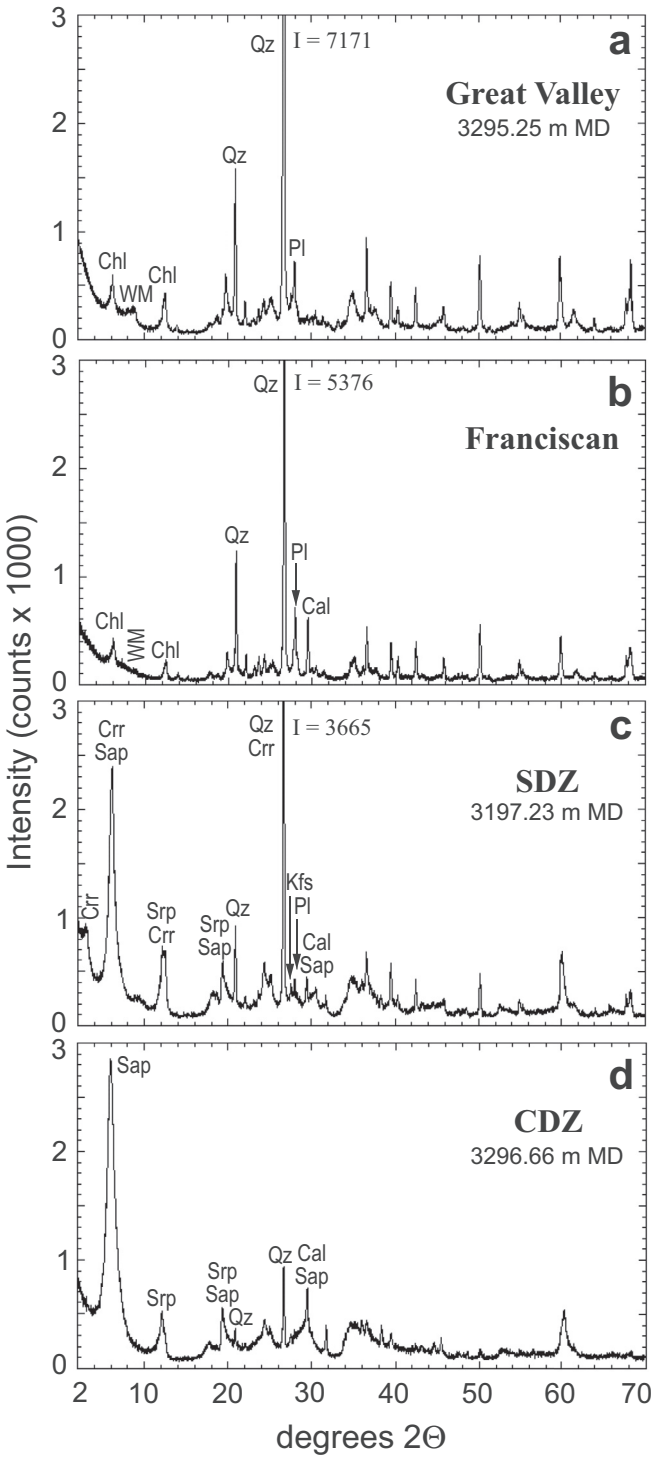

Fig. 3. X-ray diffraction (XRD) data for the SAFOD and Franciscan materials used in the friction experiments. a) Great Valley sequence; b) Franciscan mélange; c) SDZ; d) CDZ. Mineral abbreviations, after Whitney and Evans (2010): Cal, calcite; Chl, chlorite; Crr, corrensite; Kfs, K-feldspar; WM, white mica (illite and illite-smectite in a, phengite in b); Qz, quartz; Pl, plagioclase. I = intensity of quartz (101) peak at 26.65° 2Θ. Mineral identifications were verified using scanning electron microscope and electron microprobe techniques.

serpentine, in the fine-grained matrix. Therefore, to better understand the contribution of saponite to the frictional behavior of the CDZ and SDZ, saponite-bearing rocks were acquired from two locations in Scotland, Trotternish, Isle of Skye and Torbermory, Island of Mull (obtained from Mineralogical Research Co.). At both locations, the saponite fills amygdules in altered basalts; saponite from Skye has been described by Mackenzie (1957). A mineral separate was prepared by hand-picking the clays from the amygdules and separating them from the zeolites that line the vug walls. The separate was disaggregated and sieved to <90 μm size, and its identity and purity were verified by XRD analysis of an untreated and subsequently glycolated sample (Supplementary Fig. 1). The published saponite friction experiment (Lockner et al., 2011) used this synthetic gouge material. The composition of the Trotternish saponite, obtained using electron microprobe techniques, is presented in Supplementary Table 1, along with the average compositions of CDZ and SDZ saponites analyzed from depths near those of the tested gouges (Moore, 2014). Calcium accounts for roughly 70% of the interlayer charge and sodium most of the remainder in all three saponites. Behnsen and Faulkner (2013) found that the frictional strength of the dioctahedral smectite clay, montmorillonite, varies with the type of interlayer cation present. Even if their results are applicable to saponite, the Scottish saponite should be a good indicator of the frictional properties of saponite in the SAFOD gouges because of their similar interlayer-cation contents.

3. Experimental methods

This study focuses on the responses of the different materials to changes in temperature and velocity. Because of the limited supplies of the three SAFOD samples, experiments were run at a single effective normal stress. Lockner et al. (2011) observed no trends in μ or the velocity dependence of μ and effective normal stress in the range 40–200 MPa for those samples at room temperature. The four synthetic gouges prepared from bulk rock specimens were tested at temperatures in the range 25–250 °C and at axial velocities of 0.001–10.0 μm/s (corresponding sliding velocities along the sawcut are 0.00115–11.5 μm/s). The slowest velocity tested corresponds to a shearing rate of 36.4 mm/yr along the sawcut, which is close to the slip rate of the SAF in central California. Only three saponite experiments could be conducted with the very small saponite sample, at temperatures of 25°, 100°, and 200 °C and axial velocities between 0.001 and 1.0 μm/s. All experiments were run at 60 MPa pore-fluid pressure and 160 MPa normal stress, yielding a constant effective normal stress of 100 MPa.

We ran triaxial friction experiments (Table 1) with the sawcut sample configuration and furnace assembly illustrated in Fig. 4. Each sample consisted of an initially 1-mm thick layer of gouge smeared along a 30° sawcut in a Westerly granite cylinder (19.1 mm diameter). The sawcut surfaces were roughened with 120-grit SiC. The gouge was applied to the lower driving block as a thick paste prepared with the same synthetic "brine" approximating in situ groundwater chemistry at SAFOD that was used by Lockner et al. (2011) and Morrow et al. (2014). Because of concerns about corrosion, deionized water was used in the pore-pressure system for the triaxial machine. However, raising the confining pressure will cause fluids to be expelled from the compacting gouge layer, and dilution of the pore fluids with water from the pore-pressure lines may be minor. The starting fluid chemistry will be modified during an experiment as functions of the temperature and mineral assemblage being tested.

Argon gas was used as the confining pressure medium. The pore-pressure lines were evacuated for 15–20 min, during which time the confining pressure was increased to 70–80 MPa. The 60 MPa fluid pressure was then applied and confining pressure raised concurrently to 160 MPa at room temperature or ~130–140 MPa for heated experiments. In the latter case, the starting value of 160 MPa confining pressure was attained as the sample heated. Normal stress was kept constant during an

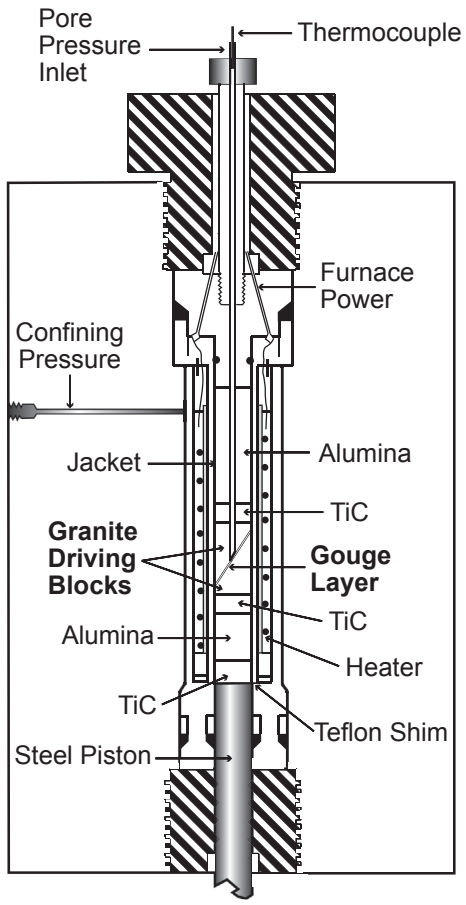

Fig. 4. Furnace assembly for triaxial friction experiments. The granite driving blocks were positioned in the jacket using alumina insulating pieces of appropriate lengths, such that the sawcut was centered over the temperature maximum of the cylindrical furnace. Temperature was 2% lower at the ends of the granite cylinders. During experiments at elevated temperatures, a circulating cooling-water system maintains the pressure vessel surrounding the furnace at room-temperature conditions.

experiment by applying changes to the confining pressure. Additional information about the sample assembly and procedures are presented in Moore and Lockner (2011, 2013).

Corrections for seal friction (Moore and Lockner, 2011, 2013) and for changes in contact area along the sliding surface (Scott et al., 1994; Tembe et al., 2010) were made during the experiment. After the experiment, +0.7 MPa was added to the normal stress, to account for lateral slip on a greased teflon shim (Tembe et al., 2010) positioned between the sample and the piston (Fig. 4). Corrections for jacket strength were also applied after the experiments. Lead jackets were used for the tests at ≤200 °C, and copper for those at 250 °C. Lead-jacket corrections are discussed in Moore and Lockner (2011) and Cu-jacket corrections in Moore and Lockner (2008). Errors in the stress calibrations or the determinations of seal friction and contact area are partly cancelled in the calculation of μ (ratio of shear stress to normal stress). The uncertainty in determining absolute coefficient of friction at this normal stress is about ±0.02 for Pb-jacket experiments and ±0.03 for those using Cu jackets (Moore and Lockner, 2013). Because tests were performed with identical procedures and jacket materials, relative variations in strength corrections between experiments should be much smaller. Furthermore, coefficient of friction differences measured for velocity steps in individual experiments are accurate to approximately ±0.001.

Selected run products were analyzed using XRD and microscopic techniques (Table 1). Covered thin sections showing the gouge layers in cross section were examined with a petrographic microscope. In other cases, the sample was separated along the sawcut and oriented fragments of gouge extracted for analysis with a scanning electron microscope (SEM).

4. Results

4.1. Strength data

Plots of coefficient of friction, μ, versus displacement for the experiments conducted on the Great Valley, Franciscan, SDZ, and CDZ samples are presented in Figs. 5 and 6. The velocity sequence in a given experiment is reported in terms of axial velocities within each figure; both axial and shear displacements are indicated on the horizontal axes. Because of the tendency for early failure of the copper jackets, velocity was stepped manually after smaller displacements during the 250 °C experiments (Fig. 6) compared to those at 25–200 °C (Fig. 5), in order to maximize the number of velocity steps in an experiment. To allow for direct comparison, the 250 °C strength data at two velocities are compared with those at 25–200 °C in Fig. 7. The first six velocity steps occur in the same sequence in all experiments, and the second interval at 0.01 μm/s is compared to the subsequent one at 1.0 μm/s. Individual strength data and the displacements at which the strengths were measured are presented in Supplementary Table 2. Plots of μ versus displacement for the saponite experiments are presented in Fig. 8. The samples separate into three groups: 1) Great Valley and Franciscan, 2) SDZ and CDZ, and 3) saponite, which will be described in turn.

4.1.1. Great Valley and Franciscan

Increasing temperature from 25° to 150 °C has little effect on the frictional strengths of either the Great Valley or Franciscan samples (Fig. 5a and b). Over the tested velocity range at these temperatures, $\mu \approx 0.40 \pm 0.03$ for the Great Valley and $\mu \approx 0.45 \pm 0.05$ for the Franciscan, with modest strain hardening. Lockner et al (2011, their Fig. 1). reported a room temperature value of $\mu = 0.43$ for this same Great Valley material at 1 μm/s axial displacement rate, consistent with the equivalent data in Fig. 5a. Similarly, Morrow et al (2010, their Fig. 3). measured $\mu \approx 0.45–0.50$ for the Franciscan mélange at room temperature, at axial velocities between 0.01 and 1.0 μm/s. In this 25–150 °C range, increasing velocity is accompanied by at least a slight increase in strength, except for the slowest step in the 150 °C Franciscan experiment.

Results at 200 °C shift to higher values of μ for both rock types. At all velocity steps except the one at 0.1–1.0 μm/s, strength is lower at the higher shearing rate. For both rocks, the highest values of μ (>0.5) were measured at 250 °C, and stick-slip events occurred at the slowest velocities. The effect of temperature on μ is seen more clearly in Fig. 7a and b. The strengths at 200° and 250 °C are greater than at lower temperatures, but the increase in μ with increasing temperature is substantially greater at the lower velocity. The coefficient of friction increases by ~0.15 for the Great Valley sample and by ~0.1 for the Franciscan sample between 25 and 250 °C at 0.01 μm/s, whereas the increase is only about half as great at 1.0 μm/s. Whereas all of the 25–150 °C strengths are higher at the higher velocity the reverse is true at 200° and 250 °C for the Great Valley sample and at 250 °C for the Franciscan one. Velocity effects will be considered in more detail later.

4.1.2. SDZ and CDZ

Results of the CDZ and SDZ experiments differ substantially from those conducted on the Great Valley and Franciscan rocks (Figs. 5–7). For one thing, $\mu < 0.2$ at all tested conditions. The CDZ and SDZ gouges respond differently to increasing temperature from

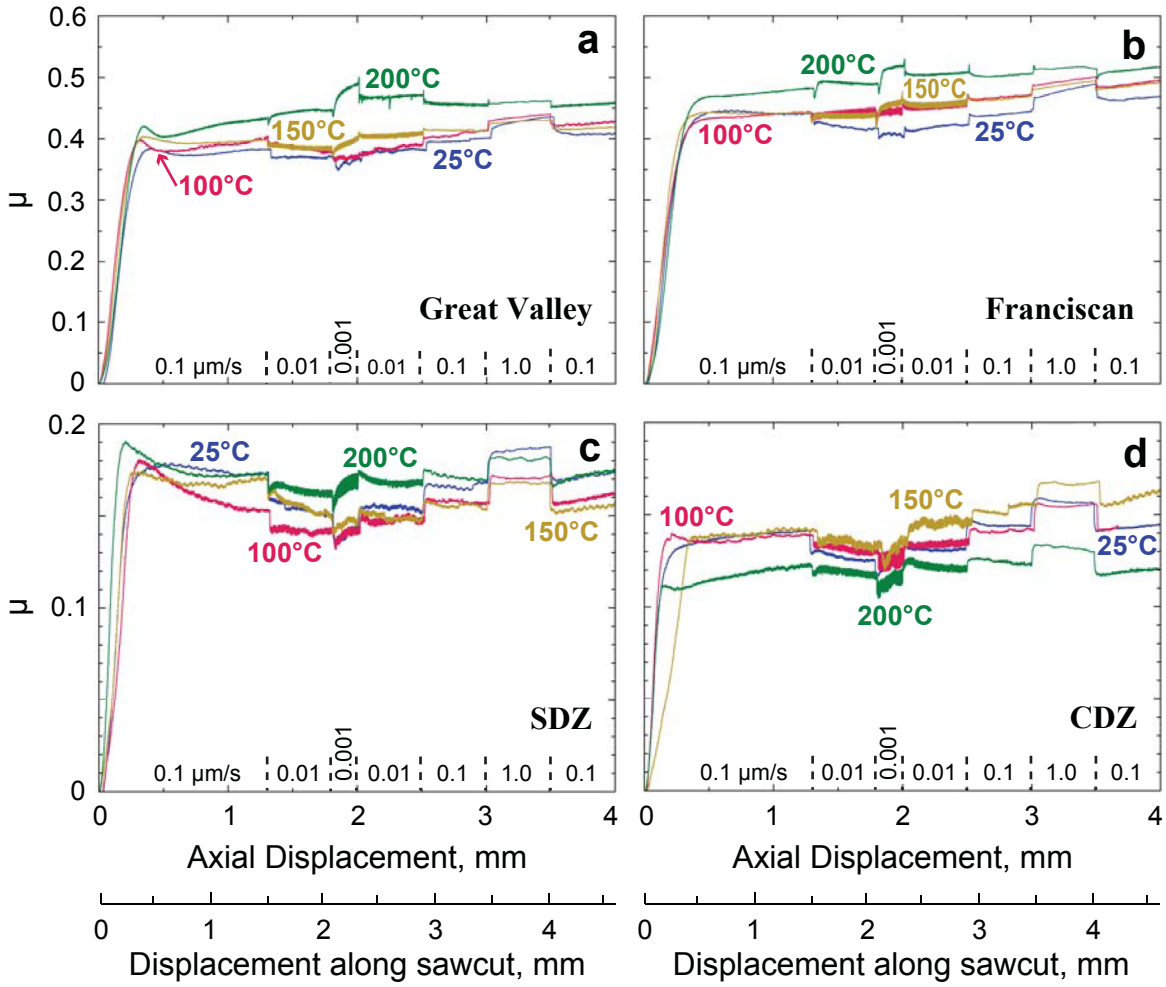

Fig. 5. Frictional strength data (Pb-jacket experiments) at temperatures in the range 25–200 °C for a) Great Valley sequence, b) Franciscan Complex mélange, c) SDZ, and d) CDZ samples. The sequence of axial velocities tested is at the bottom of each plot.

the Great Valley and Franciscan samples, and they also behave somewhat differently from each other. All of the measured SDZ strengths lie in the same narrow range of $\mu = 0.14–0.19$, and there is no discernible trend in μ with increasing temperature to 250 °C (Fig. 7c). The CDZ results at 25°, 100°, and 150 °C largely overlap (Fig. 5d), whereas the 200° and 250 °C data are shifted to progressively lower values of μ (Fig. 7d). In the temperature range 25–150 °C, μ for the CDZ gouge varies between 0.12 and 0.17 over the range of velocities tested, whereas at 200 °C the range narrows to 0.11–0.13 and at 250 °C it is 0.08–0.13 at velocities between 0.001 and 1.0 μm/s.

For every velocity step in Figs. 5d and 6d, the strength of the CDZ gouge is greater at the higher shearing rate. The same is essentially true for the SDZ gouge, although at 200° and 250 °C, μ at 0.01 μm/s axial velocity appears to be slightly lower than at 0.001 μm/s. The heated CDZ and SDZ strength data, along with the saponite data in Fig. 8, are characterized by oscillations in μ that become more pronounced at the slower sliding velocities. This is not a material property, but rather noise in the data generated by temperature oscillations (<1 °C) that lead to changes in sample column length and ultimately to stress oscillations (for example, at 0.001 μm/s in Fig. 5c and d). The cycling occurs in all of the heated experiments, but it is most obvious in those conducted on very weak materials.

Great care was taken to determine strength corrections for both Pb and Cu jackets as a function of temperature and total slip. The largest shear strength corrections were 7.5 MPa for Cu jackets by 3 mm displacement and represented an adjustment of $\mu = -0.075$. Ultimately, the change in jacketing material in the 250 °C experiments does not appear to affect the results. All of the trends in strength identified in the 25–200 °C experiments (Fig. 5) continue at 250 °C (Figs. 6 and 7).

4.1.3. Saponite

At room temperature saponite is extremely weak; $\mu = 0.05–0.07$ over the velocity range tested (Fig. 8), consistent with the strength reported by Lockner et al. (2011) for the same gouge. Room-temperature strength increases with increasing velocity, and there is no obvious strain hardening. On the other hand, the two heated samples are characterized by strain hardening after the first velocity change, except for shear at the slowest velocity at 200 °C. The lowest strength, $\mu = 0.04$, was measured at 200 °C, 0.001 μm/s, and the highest was $\mu = 0.085$ at the end of the 100 °C experiment.

4.2. Velocity data

At each velocity step, the change in μ, $\Delta\mu_{ss}/\Delta\ln V = (a–b)$ was determined and the error estimated. For velocity stages characterized by stick slip (e.g., Fig. 6a), strength was averaged over the displacement interval where the stress drop was smallest. The data were detrended to remove strain-hardening effects before making

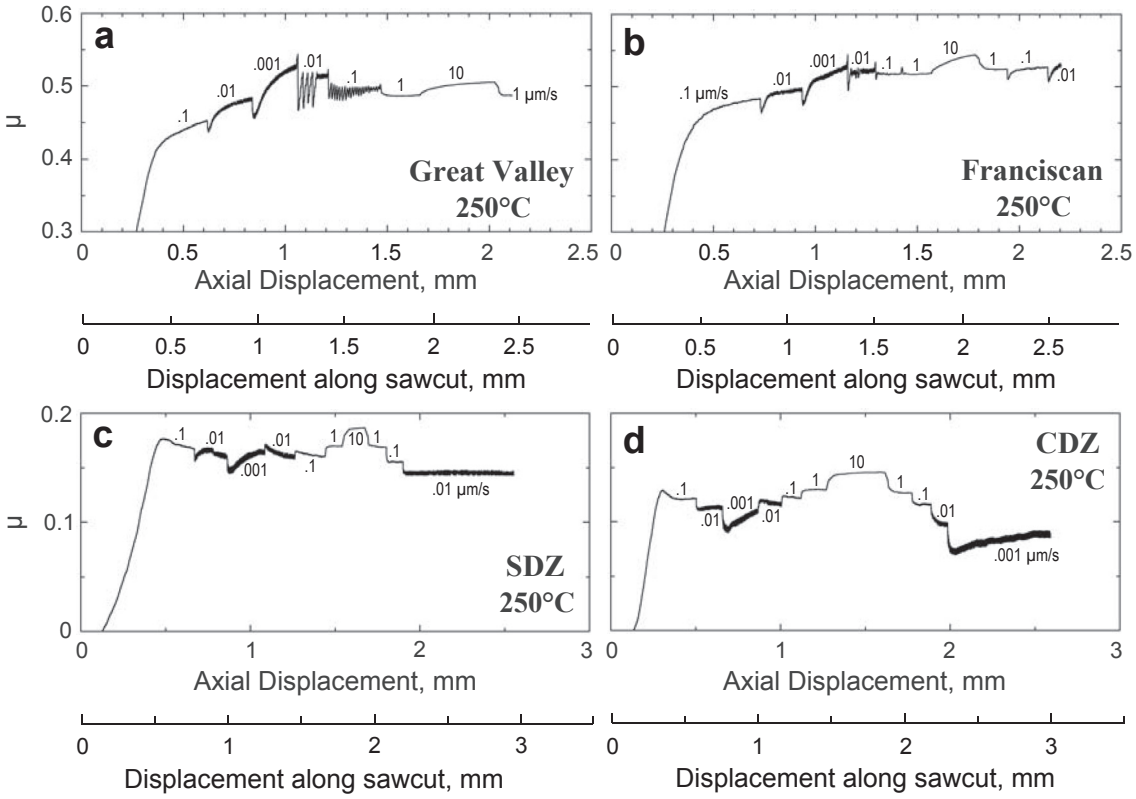

Fig. 6. Frictional strength experiments at 250 °C, using Cu jackets, for a) Great Valley, b) Franciscan, c) SDZ, and d) CDZ samples. The axial velocity of each step is identified on the plots.

the determinations. Corrections for the velocity dependence of seal friction and of the Cu-jacket strength were made as outlined in Appendix A of Moore and Lockner (2013). The Pb-jacket strength was found to be independent of velocity (Moore and Lockner, 2011).

Plots of (a-b) versus the log of axial velocity from all of the experiments are presented in Figs. 9 and 10. Data are plotted at the midpoint of the velocity step (e.g., at −1.5 for the velocity step between 0.01 and 0.1 μm/s, both up-steps and down-steps). Because of overlaps, some data points are shifted slightly to the right to make them visible. All of the data and accompanying error estimates are presented in Supplementary Tables 3–7. Error bars are left out of the figures to avoid clutter. Typical uncertainty is on the order of 10^{-4} for the room-temperature experiments and the highest-velocity steps at elevated temperatures, whereas the temperature-based oscillations that are prominent at low velocities raise uncertainty by as much as an order of magnitude.

Although there is some scatter in the Great Valley and Franciscan data (Fig. 9a and b), (a-b) for both materials decreases with decreasing velocity and increasing temperature. For the Great Valley sample, (a-b) $\geq$ 0 throughout the temperature range 25°–150 °C, whereas (a-b) < 0 at the two slowest velocity steps of the 150 °C Franciscan experiment. At 250 °C, only the fastest velocity step (1–10 μm/s, not tested at lower temperatures) yielded (a-b) > 0 (Fig. 9a and b).

The CDZ velocity data differ substantially from the Great Valley and Franciscan results in that (a-b) > 0 at all tested conditions and there is no obvious correlation with either velocity or temperature (Fig. 9d). The SDZ, however, does show some similarities to the Great Valley and Franciscan samples, in that (a-b) decreases with decreasing velocity and increasing temperature (Fig. 9c). However, the furnace-induced noise makes the determinations of (a-b) somewhat uncertain at the slowest velocities. As was observed with the strength data, in all cases the (a-b) values at 250 °C obtained using copper jackets continue trends established at lower temperatures.

The pure saponite gouge is velocity strengthening at all tested conditions (Fig. 10). The highest-velocity step at 25 °C has the largest value of (a-b) ~ 0.0040; all other (a-b) values cluster in a narrow range between ~0.0010 and ~0.0025.

4.3. Petrography and mineralogy

Thin sections provide views across the thickness of the gouge layer (Fig. 11), whereas the SEM photos typically show the shear surfaces (Fig. 12). Shear in all examined samples is concentrated in subsidiary traces, predominantly B and R shears in the Franciscan and Great Valley samples (Fig. 11a and b) and also including Y and numerous P shears in the SDZ and CDZ (Fig. 11c and d). Subsidiary-shear terminology is from Logan et al. (1979). Both P and R shears also formed in water-saturated CDZ gouge samples tested by French et al. (2015). Moore and Byerlee (1991) measured the orientations relative to fault strike of mapped recently active breaks along the length of the SAF. They found that P-oriented traces were more abundant in the creeping than the locked fault sections, consistent with the concentration of P shears in the SDZ and CDZ gouges.

There is a textural progression among the gouges related to their phyllosilicate contents. On the one hand, for the more quartz- and feldspar-rich Great Valley and Franciscan rocks, the gouge between shears is relatively undeformed and lacking in fabric (Fig. 11a and b). The individual shears have variable thicknesses, and in thin section they are seen to be composed of multiple sub-parallel layers. This is also illustrated in Fig. 12a and b, which look down on a B shear. The modestly slickensided surface (Fig. 12a) has some depth to it, exposing progressively lower levels moving from

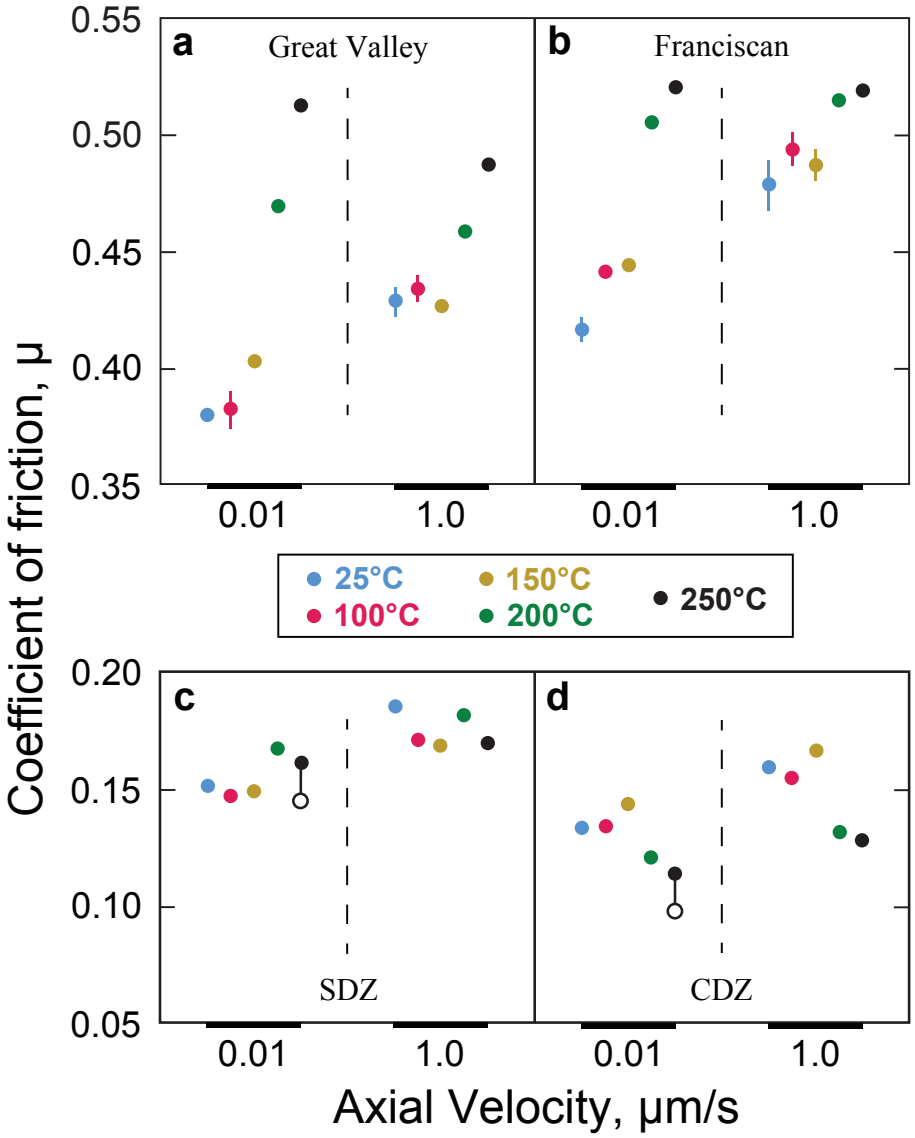

Fig. 7. Comparison of 250 °C (Fig. 6) and 25–200 °C (Fig. 5) strength data for the a) Great Valley, b) Franciscan, c) SDZ, and d) CDZ samples at 0.01 and 1.0 μm/s axial velocities. Filled circles compare the second interval at 0.01 mm/s to the subsequent step at 1.0 μm/s. Open circles are for a third step at 0.01 μm/s with different μ. In most cases, the spot size equals or exceeds the measured range of μ; vertical bars indicate wider ranges. The plotted strength data are listed in Supplementary Table 2, along with the displacements at which the measurements were made.

bottom to top of the image. The irregular white bands in the image mark the changes in elevation (edge effects). The step outlined by the box is shown at higher magnification in Fig. 12b. The exposed edge reveals a stack of sub-parallel layers. The slickensides develop in smears of very fine-grained material, but numerous larger, equant grains (to a few μm in diameter) are visible immediately below the surface. Energy Dispersive Spectroscopy (EDS) spot analyses made on the smooth, slickensided surfaces of the Franciscan and Great Valley samples indicate a mixture of minerals in varying proportions (Supplementary Fig. 2).

The very phyllosilicate-rich SDZ and CDZ run products (Fig. 11c and d) exhibit a more complicated network of subsidiary shears that, combined with the development of a clay fabric in the lozenges of gouge between them, produce an anastomosing texture that mimics the natural fault gouge (Fig. 2c and d). The shear planes are much smoother and more extensively slickensided than those in the Franciscan and Great Valley samples (compare Fig. 12c with Fig. 12a and b). The slickensided surfaces generated in the CDZ gouge during the experiments (Fig. 12c) have the composition of saponite (Supplementary Fig. 3), and they closely resemble the natural slickensides found in the SAFOD gouges (Fig. 12d).

Other than the presence of shinier shear surfaces in the 250 °C run products, there were no major textural changes with increasing temperature. Except for the 10-day CDZ experiment at 250 °C (Fig. 6d), all of the tests lasted between 3 and 4 days. No changes in mineral assemblage were identified in any of the bulk XRD analyses of the run products. In particular, neither the corrensite in the SDZ nor the saponite in the mineral separate and the foliated gouges was affected by heating.

5. Discussion

5.1. Comparison of Great Valley and Franciscan results with similar crustal rock types

The tested Great Valley sequence and Franciscan Complex

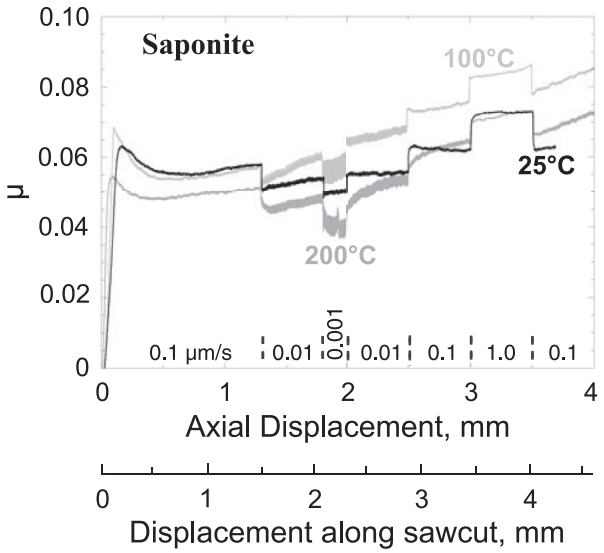

Fig. 8. Saponite frictional strength at 25°, 100°, and 200 °C, using Pb-jacketed samples. The velocity sequence is indicated at the bottom of the plot. The spike in strength midway through the slow step at 200 °C (~1.9 mm) was caused by a change in laboratory room temperature.

samples are both characterized by modest increases in strength at T > 150 °C and a progressive change from purely velocity-strengthening behavior at T ≤ 100 °C to largely velocity-weakening behavior and stick slip at 250 °C. Similar responses to changing temperature and velocity have been observed in a number of other phyllosilicate-bearing quartzofeldspathic rocks, as documented in recent studies. Boulton et al. (2014) measured the frictional properties of fault gouge samples retrieved from shallow drillholes through the principal slip zone of the Alpine Fault of New Zealand. The two tested gouges are altered amphibolite-facies mylonites of the Alpine Schist; one contains ~16% phyllosilicates (9% muscovite/illite, 7% chlorite) and the other one ~32% phyllosilicates, largely montmorillonite. With increasing temperature, both gouges become stronger and change from predominantly velocity-strengthening to velocity-weakening (T ≥ 140 °C) and stick-slip (T ≥ 210 °C) behavior. The montmorillonite-rich gouge displays both a significantly greater temperature-related strength increase and a transition to velocity weakening at lower pressure-temperature conditions than the gouge containing white mica and chlorite.

Tembe et al. (2009) reported heated frictional strengths of an illite-rich (≥50% illite + mixed-layer clays) "black gouge" from a ~30 cm-wide shear zone recovered in a SAFOD Phase 1 spot core (3067 m MD in the main hole). This minor, inactive fault is located at the contact between a siltstone and an arkosic sandstone in the Pacific Plate. The black gouge has a coefficient of friction, μ~0.4 between 25 and 200 °C, but it strengthens considerably at higher temperatures, reaching μ > 0.7 at 430 °C. The gouge is velocity weakening at temperatures above ~250 °C, in some cases accompanied by oscillatory or stick-slip motion. den Hartog et al. (2012) investigated velocity and temperature dependence of a shale containing approximately 60% illite, 25% quartz, and 15% chlorite. The room-temperature illite-rich gouge was velocity strengthening, whereas the heated samples were stronger and also showed a transition to largely rate-weakening behavior by 300 °C. den Hartog and Spiers (2013) determined that the range over which velocity weakening occurs in illite-quartz mixtures is a function of temperature, effective normal stress, mineral proportions, and sliding velocity.

The results of these other studies are consistent overall with the Great Valley and Franciscan data, although the illite/montmorillonite-rich gouges strengthen to a greater degree with heating than the somewhat more chloritic Great Valley and Franciscan rocks. Notably, all of these studies combined suggest that high phyllosilicate contents in quartzofeldspathic rocks are no guarantee of stable slip in the seismogenic zone of the continental crust, particularly at the deeper levels where major earthquakes typically nucleate.

5.2. Saponite and the frictional strengths of the CDZ and SDZ

Water-saturated saponite may be the weakest mineral that has been identified to date; only talc at 300 °C has comparably low strength at high effective normal stresses (Moore and Lockner, 2008). Montmorillonite with similar interlayer-cation contents (Ca > Na) would be approximately twice as strong as saponite at room temperature and comparable effective stress (Behnsen and Faulkner, 2013). The very small number of experiments (Fig. 8) conducted on the saponite separate limits the conclusions that can be drawn from the data. An added complication is the strain hardening shown by the heated samples, the cause of which is unknown. Prior to the onset of the strain hardening (≤1.5 mm, Fig. 8), the 25° and 100 °C results coincide while strength is lower at 200 °C. Such temperature-related strength behavior is consistent with that of the saponite-rich CDZ gouge (Figs. 5d and 6d).

In most natural occurrences, saponite is stable only at relatively low temperatures. In some burial depositional environments, saponite alteration can begin at temperatures <100 °C, whereas it is stable to 150°–200 °C in active geothermal systems (Kristmannsdottir, 1979; Schiffman and Fridleifsson, 1991; Robinson et al., 2002). However, saponite has been synthesized stably on its own composition at temperatures as high as 850 °C (Iiyama and Roy, 1963; Kuchta and Fajnor, 1988), indicating that it can persist to higher P-T conditions in rocks of suitable chemistry. Examples include the assemblage saponite + phlogopite + tremolite + diopside which formed during prograde metamorphism of magnesian limestone (Wilson and Bain, 1970), and iron-rich saponite that crystallized as a late-stage, subsolidus (T < 600 °C) replacement of fayalitic olivine in a plutonic body (Mücke, 2003).

The XRD analyses indicate that the saponite in the CDZ and SDZ gouges was unaffected by heating to 250 °C for as long as 10 days, and this mineral has a major influence on the laboratory friction data obtained for the CDZ and SDZ. The higher strengths of both the CDZ and SDZ gouges compared to pure saponite are consistent with mixing-law studies on mixtures of quartz and phyllosilicate minerals. Specifically, the experiments of Tembe et al. (2010) on a mixture of montmorillonite + illite + quartz correspond most closely to the saponite + serpentine + quartz/feldspar assemblages of the CDZ and SDZ. Weakening of the ternary mixture was greater than would be calculated by averaging the two binary quartz-clay mixtures tested by Tembe et al. (2010), indicating that the weaker montmorillonite has a greater influence on strength than the stronger illite. Adding ~20% quartz to the montmorillonite/illite mixture raised μ by ~0.05–0.06 and ~40% quartz raised μ by ~0.10–0.12 relative to the pure montmorillonite sample tested by Tembe et al. (2010). Such increases in the ternary mixtures are consistent with the differences in strength between pure saponite and the CDZ and SDZ, respectively.

Saponite dominates the mineralogy of the CDZ and, as discussed above, it can explain the very low strength of this gouge and its weakening at T ≥ 150 °C. More sensitive friction experiments conducted on the CDZ gouge by Coble et al. (2014) and French et al. (2015) suggest that the weakening may extend to temperatures as

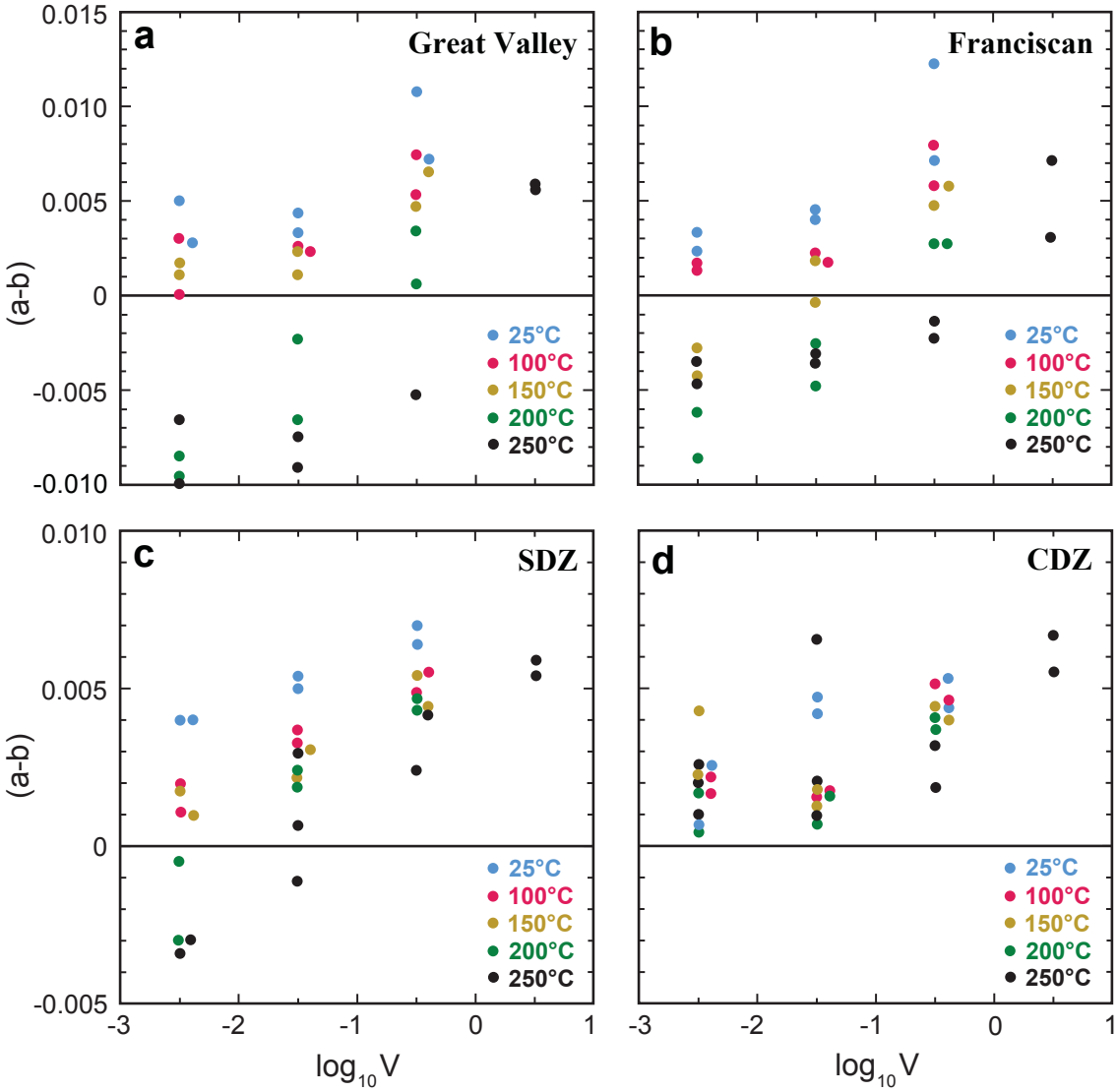

Fig. 9. Summary of velocity data, (a–b), in the temperature range 25°–250 °C for a) Great Valley, b) Franciscan, c) SDZ, and d) CDZ samples. Data are plotted at the midpoints of velocity steps; some data points are shifted slightly to improve visibility. All of the data and error estimates are presented in Supplementary Tables 3–6.

low as 80–120 °C. The temperature-weakening, velocity-strengthening behavior indicated for saponite from these experiments corresponds to that described previously for talc (Moore and Lockner, 2008), and the two minerals are related both crystallographically and chemically. Saponite is a 2:1 trioctahedral sheet silicate that is modified from the talc [$Mg_3Si_4O_{10}(OH)_2$] structure by the replacement of some Si^{4+} with Al^{3+}, coupled with the addition of interlayer cations to balance the charge (Supplementary Table 1). The similar frictional behavior of these two minerals may be a function of their closely related crystal structures, in particular the nature of their (001) bonds. In contrast, the frictional properties of the smectite clays montmorillonite and saponite appear to trend in opposite directions with heating. Of the two Alpine Fault gouges tested by Boulton et al. (2014), the montmorillonite-rich sample was ~30% weaker at room temperature than the one containing muscovite/illite and chlorite, but it was stronger at $T \geq 140$ °C. The transition from velocity strengthening to velocity weakening also occurred at lower temperatures for the montmorillonite-bearing gouge. Montmorillonite is a dioctahedral smectite clay, and dioctahedral 2:1 sheet silicates are stronger than their trioctahedral equivalents at room temperature (Moore and Lockner, 2004; Behnsen and Faulkner, 2012). To date, however, the comparative effects of increasing temperature on these two minerals have not been systematically investigated. The possibility that the individual smectite clays respond differently to heating should be tested in future studies.

Saponite-rich gouges very similar to the CDZ from two other fault zones have recently been reported and tested in room-temperature friction experiments. In both occurrences, one in New Zealand (Barth et al., 2013) and one in Japan (Sone et al., 2012), the saponite-rich gouge was produced by the reaction of serpentinite with crustal rocks, the same as for the SAFOD creeping traces (e.g., Moore and Rymer, 2012). The saponite-chlorite-lizardite gouges tested by Barth et al. (2013) from the southern Alpine Fault had coefficients of friction of 0.12–0.13. Sone et al. (2012) reported $\mu = 0.06$–0.12 for the saponite-rich gouge from Japan.

Although much more closely aligned with the CDZ, the SDZ to some extent behaves in a manner intermediate between the temperature-weakening and velocity-strengthening CDZ and temperature-strengthening and velocity-weakening Great Valley-

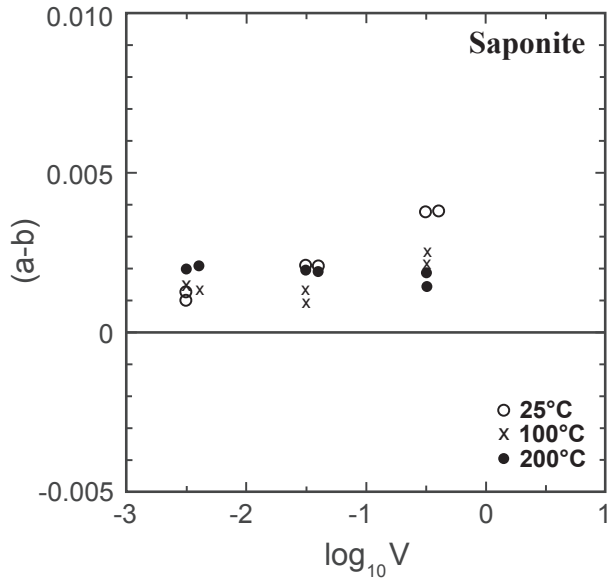

Fig. 10. Velocity data for saponite. Individual data and error estimates can be found in Supplementary Table 7.

Franciscan rocks. Its strength does not change with increasing temperature, and it is characterized by negative (a-b) values at the slowest-velocity and highest-temperature conditions tested. The behavior of the SDZ sample can be explained by its higher quartz and feldspar contents compared to the CDZ (Fig. 3). The SDZ gouge also contains the Mg-clay mineral corrensite (Moore, 2014), but its frictional properties are as yet unknown. Corrensite is a structurally ordered mixed-layer clay consisting of alternating layers of saponite and chlorite, and the saponite layers may influence the physical properties of corrensite.

The associations of temperature-strengthening with velocity-weakening behavior and of temperature weakening with velocity strengthening for these gouges are consistent with those reported in many other studies. For quartz-rich gouges, changes in the dominant friction mechanism operative at different P-T conditions define the depth extent of the seismogenic zone in crustal faults (e.g., Chester, 1995). The Great Valley and Franciscan data are consistent with the Chester (1995) rheological model, whereas other processes dominate in the saponite-rich gouges (Moore and Lockner, 2013). As illustrated by the intermediate behavior of the SDZ gouge, there may be a gradual transition over a range of mineral proportions. Detailed microstructural and laboratory investigations are required to elucidate the variations in frictional mechanisms over P-T-composition space.

5.3. Implications for the San Andreas creeping section

The strength data at 100° and 150 °C plotted in Fig. 5 are essentially the same as those at room temperature, indicating that the room-temperature strengths reported previously for these rock types are valid to 3–4 km depth. These low-temperature data highlight the marked differences in strength between the creeping traces and major lithologic units associated with the SAF in central California (Fig. 1c). At higher temperatures these differences are magnified, as the behavior of the Great Valley and Franciscan rocks diverges from that of the creeping traces. As temperature rises above ~150 °C, the Great Valley and Franciscan rocks strengthen and become velocity weakening over a progressively wider range of velocities. They also undergo the laboratory equivalent of earthquakes at 200–250 °C. Mineral assemblages and compositions of the tested Great Valley sample suggest that it underwent diagenesis at temperatures of ~175°–200 °C and burial depths of 5–6 km (Moore, 2014) consistent with the temperature estimates for Great Valley core from the bottom of the main SAFOD borehole (Schleicher et al., 2009). Mineral assemblages of Central belt Franciscan rocks indicate subduction to depths of ~15–18 km at temperatures of 150–250 °C (e.g., Ernst and McLaughlin, 2012). The mineral assemblages of the Franciscan and Great Valley samples, therefore, are stable over the 150°–250 °C range where the frictional properties change, and further increases in P-T conditions to the base of the seismogenic zone at ~350 °C should have little effect on mineralogy. These and similar rock types will promote earthquakes, not stable slip, throughout the seismogenic zone, as illustrated by present-day deformation NE of the central SAF.

As stated previously, the tested Great Valley and Franciscan samples were chosen for study because of their relatively high phyllosilicate contents. The more quartz- and feldspar-rich rocks in the Hole G core (e.g., Bradbury et al., 2011; Holdsworth et al., 2011) are stronger at room temperature (Lockner et al., 2011) and also probably capable of generating earthquakes at depth, as has been demonstrated in laboratory experiments on quartzite (Chester and Higgs, 1992) and granite (Blanpied et al., 1995).

Present-day relative plate motion across the San Andreas Fault system in central California is characterized by oblique convergence (e.g., Pollitz, 1986; Atwater and Stock, 1998). Titus et al. (2011) estimated a fault-perpendicular shortening rate of ~5.4 mm/yr in this area, and most of the deformation, with accompanying seismicity, is concentrated in the Diablo Range NE of the creeping section on Franciscan-Great Valley basement. The blind thrust faults beneath the Coalinga and Kettleman Hills anticlines (Fig. 1c), for example, were characterized by $5.5 \leq M_w \leq 6.5$ earthquakes in 1982 (New Idria), 1983 (Coalinga) and 1985 (Kettleman Hills) (e.g., Eaton, 1990; Ekström et al., 1992; Stein and Ekström, 1992). Titus et al. (2011) concluded that the ~30 mm/yr maximum creep rate measured in the San Andreas creeping section (Titus et al., 2006) is consistent with long-term slip rates on the Carrizo Plain segment based on paleoseismological estimates (Noriega et al., 2006). In consequence, accumulation of elastic strain is not required for the central part of the creeping section.

French et al. (2014) conducted high-speed friction experiments on CDZ gouge in a rotary-shear apparatus. In contrast to its velocity-strengthening behavior at low velocities, water-saturated CDZ gouge weakens with increasing velocity between 0.1 and 1.3 m/s. They attributed the weakening in large part to a combination of slip localization and thermal pressurization of pore fluids. Within the limitations of extrapolating the laboratory results to the SAF, they concluded that nucleation of a sizable earthquake in the CDZ was unlikely, although a Parkfield-type earthquake could possibly propagate through it.

The heated CDZ data could explain the continued weakness and stable slip of the creeping section in terms of a mineralogical control. In contrast to the Great Valley and Franciscan rocks, however, the mineralogy of the creeping traces probably is different at depths greater than 3–4 km. Although saponite potentially could be stable throughout the seismogenic zone under appropriate lithological conditions, as discussed previously, the presence of corrensite in the SDZ and, to a much lesser extent the CDZ (Moore, 2014), suggests that this is not the case here. The replacement of saponite by corrensite is estimated to begin at ~125 °C (Moore, 2014), based on occurrences in the Coast Range ophiolite (Evarts and Schiffman, 1983; Bettison and Schiffman, 1988). The corrensite, in turn, may be completely replaced by chlorite at ~225 °C (e.g., Evarts and Schiffman, 1983; Schleicher et al., 2009, 2012; Moore, 2014).

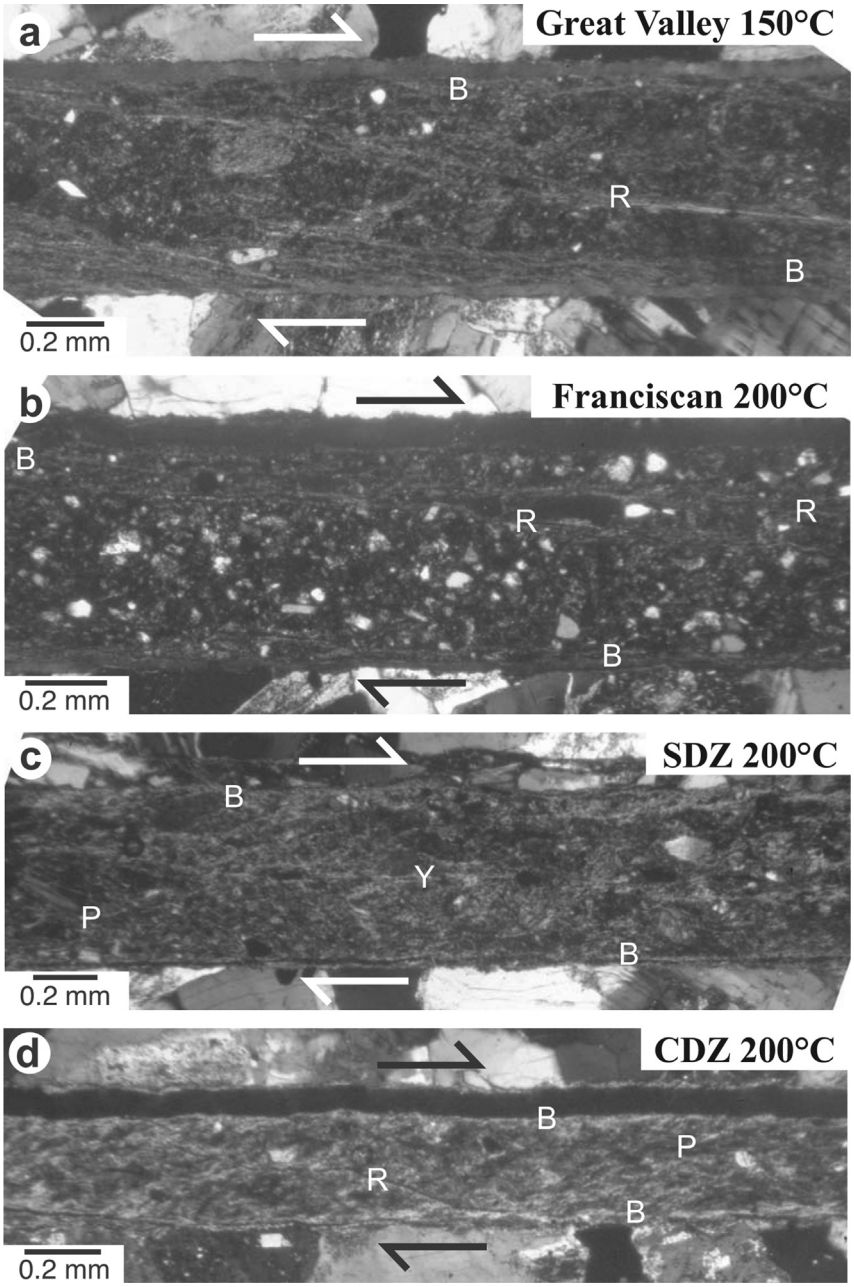

Fig. 11. Photomicrographs of thin-sectioned run products: a) Great Valley, 150 °C; b) Franciscan, 200 °C; c) SDZ, 200 °C; and d) CDZ, 200 °C. All samples are oriented to show right-lateral offset, and all photos are taken with crossed polarizers. Abbreviations: B, a shear oriented parallel to the sawcut and situated close to the boundary with the driving blocks; R, Riedel shear; P, P shear; and Y, a shear oriented roughly parallel to the sawcut and located in the center of the gouge layer.

The mineral assemblage chlorite + tremolite/actinolite + talc is characteristic of reaction zones developed between serpentinite and crustal rocks at subgreenschist-to greenschist-facies conditions ($T \geq 225$ °C; e.g., Soda and Takagi, 2010). The saponite-rich gouge studied by Sone et al. (2012) overprints an earlier, higher-temperature shear zone developed between serpentinite and metasedimentary rocks. The shear zone is mineralogically zoned, with talc + tremolite adjacent to the serpentinite and chlorite adjacent to the metasedimentary rocks. In many other reaction zones (e.g., Sanford, 1982) a monomineralic talc layer adjoins the ultramafic rocks. The SDZ and CDZ contain porphyroclasts of talc and of tremolite + chlorite (Moore and Rymer, 2012) suggesting a possible source from deeper levels of the seismogenic zone. Localization of shear within a talc-rich layer could satisfy the strength limitations of the SAF in the deeper portion of the creeping section (Moore and Rymer, 2007). The magnesium-rich chlorite associated with ultramafic rocks also is very weak, with $\mu \approx 0.2$ at temperatures to 300 °C (Moore and Lockner, 2015). A major question, however, is the depth of the serpentinite source for the fault (McPhee et al., 2004; Moore and Rymer, 2007). If the serpentinite does extend to 10–12 km depth in the fault, other unknowns would be the extent of metasomatic alteration and how the alteration minerals are distributed within the fault. In this regard, study of exhumed serpentinite-bearing faults in other areas (e.g., Japan, Sone et al., 2012) might help to delineate the character of the SAF at depth in the creeping section.

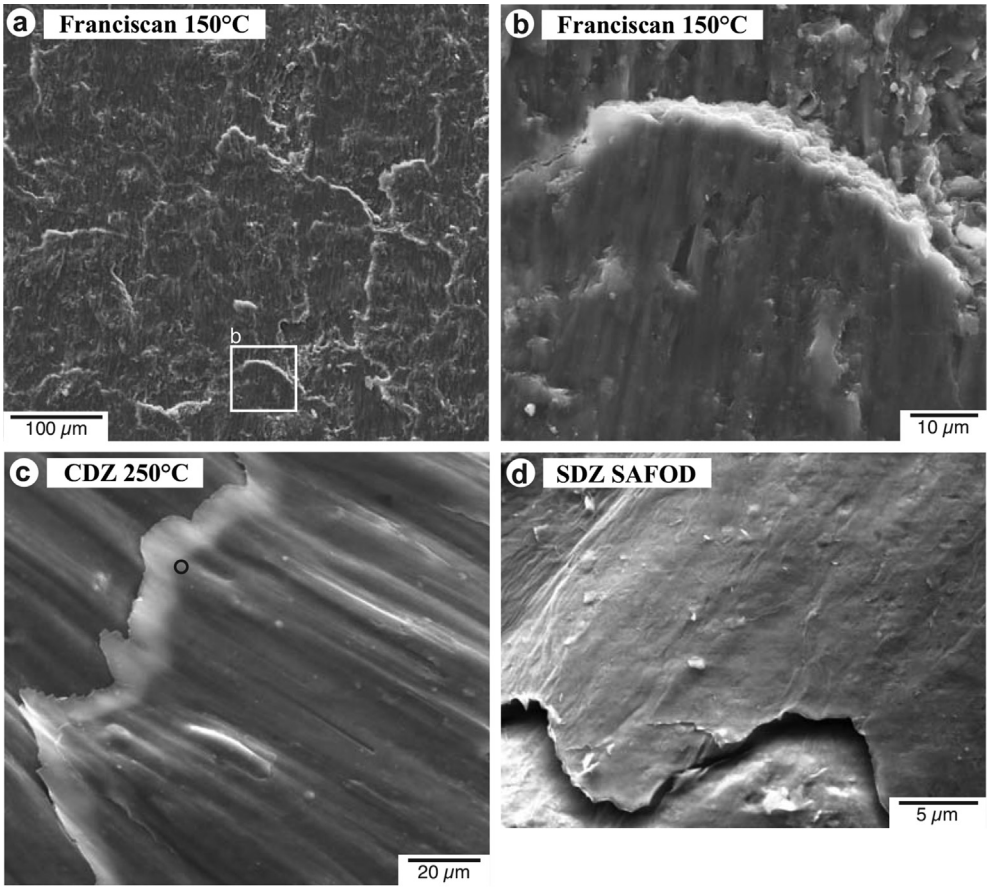

Fig. 12. Secondary-electron SEM photos of laboratory-generated and natural shear surfaces. a) Lower- and b) higher-magnification views of a somewhat slickensided boundary-shear surface developed in the Franciscan sample sheared at 150 °C. c) Well slickensided shear formed in the CDZ gouge during an experiment at 250 °C. The open circle marks the location of the energy dispersive system (EDS) spectrum in Supplementary Fig. 3. d) High-magnification image of a fragment of SDZ gouge plucked from the core at 3197.18 m MD; the SDZ photo also appears in the SAFOD Phase 3 Core Atlas (http://www.earthscope.org).

In the absence of an 8–10 km deep drillhole at SAFOD, the origin of the very low strength and stable slip of the SAF creeping section must remain speculative, including whether a mineralogical explanation is sufficient or whether additional or alternative mechanisms such as fluid overpressures (e.g., Le Pourhiet and Saleeby, 2013) are required.

6. Conclusions

Hydrothermal strength experiments conducted on Franciscan Complex and Great Valley sequence quartzofeldspathic rocks, which outcrop extensively in the Coast Ranges of central and northern California, demonstrate that their strengths increase progressively with increasing temperature above 150 °C. The strengthening is accompanied by a transition from velocity-strengthening to velocity-weakening and stick-slip behavior. The Great Valley and Franciscan frictional properties are consistent with those of similar crustal rocks characteristic of locked faults, including the locked portions of the SAF. In contrast, the two creeping traces at SAFOD, the CDZ and SDZ, have very different frictional behavior that reflects their unusual rock chemistry and mineralogy. The differences between the CDZ and the country rocks become even more pronounced at elevated temperatures as the CDZ, which is very weak and velocity strengthening at room temperature, weakens further and remains velocity stengthening at higher temperatures. Both creeping traces are rich in the smectite clay saponite, and tests on a saponite-mineral separate confirm that it is a major (SDZ) to dominant (CDZ) factor in the frictional behavior of these gouges. Although the likelihood that saponite is not present at $T \geq 150$ °C in the fault makes the applicability of the higher temperature data uncertain, substituting talc and Mg-rich chlorite for saponite could yield the same extremely low strength and stable slip, depending on their abundance and distribution in the fault. Examination of exhumed shear zones of similar lithologic character may provide clues to the nature of the SAF creeping section at seismogenic depths.

Acknowledgments

The authors thank Sharon Cisneros of Mineralogical Research Co. for her help in obtaining the Scottish saponite-bearing samples for study. Lee-Gray Bose provided laboratory assistance and Leslie Hayden helped with the SEM and microprobe work. The paper was improved by the reviews of N. Beeler, B. Kilgore, C. Collettini, and R. Holdsworth.

Any use of trade, firm, or product names is for descriptive purposes only and does not imply endorsement by the U.S. Government.

Appendix A. Supplementary data

Supplementary data related to this article can be found at http://dx.doi.org/10.1016/j.jsg.2016.06.005.

References

Atwater, T., Stock, J., 1998. Pacific-North America plate tectonics of the Neogene southwestern United States: an update. Int. Geol. Rev. 40, 375–402. http://dx.doi.org/10.1080/00206819809465216.

Bailey, E.H., Irwin, W.P., Jones, D.L., 1964. Franciscan and related rocks and their significance in the geology of western California. Cal. Div. Mines Geol. Bull. 183, 0–177.

Barth, N.C., Boulton, C., Carpenter, B.M., Batt, G.E., Toy, V.G., 2013. Slip localization on the southern Alpine Fault, New Zealand. Tectonics 32, 620–640. http://dx.doi.org/10.1002/tect.20041.

Behnsen, J., Faulkner, D.R., 2012. The effect of mineralogy and effective normal stress on frictional strength of sheet silicates. J. Struct. Geol. 42, 49–61. http://dx.doi.org/10.1016/j.jsg.2012.06.015.

Behnsen, J., Faulkner, D.R., 2013. Permeability and frictional strength of cation-exchanged montmorillonite. J. Geophys. Res. 118, 2788–2798. http://dx.doi.org/10.1002/jgrb.50226.

Bettison, L.A., Schiffman, P., 1988. Compositional and structural variations of phyllosilicates from the Point Sal ophiolite, California. Am. Min. 73, 62–76.

Blanpied, M.L., Lockner, D.A., Byerlee, J.D., 1995. Frictional slip of granite at hydrothermal conditions. J. Geophys. Res. 100 (B7), 13,045–13,064.

Boulton, C., Moore, D.E., Lockner, D.A., Toy, V.G., Townend, J., Sutherland, R., 2014. Frictional properties of exhumed fault gouges in DFDP-1 cores, Alpine Fault, New Zealand. Geophys. Res. Lett. 41 http://dx.doi.org/10.1002/2013GL058236.

Bradbury, K.K., Davis, C.R., Shervais, J.W., Janecke, S.U., Evans, J.P., 2015. Composition, alteration, and texture of fault-related rocks from Safod core and surface outcrop analogs: evidence for deformation processes and fluid-rock interactions. Pure Appl. Geophys. 172, 1053–1078. http://dx.doi.org/10.1007/s00024-014-0896-6.

Bradbury, K.K., Evans, J.P., Chester, J.S., Chester, F.M., Kirschner, D.L., 2011. Lithology and internal structure of the San Andreas fault at depth based on characterization of Phase 3 whole-rock core in the San Andreas Fault Observatory at Depth (SAFOD) borehole. Earth Planet. Sci. Lett. 310, 131–144. http://dx.doi.org/10.1016/j.epsl.2011.07.020.

Carpenter, B.M., Saffer, D.M., Marone, C., 2012. Frictional properties and sliding stability of the San Andreas Fault from deep drill core. Geology 40 (8), 759–762. http://dx.doi.org/10.1130/G33007.1.

Carpenter, B.M., Saffer, D.M., Marone, C., 2015. Frictional properties of the active San Andreas Fault at SAFOD: implications for fault strength and slip behavior. J. Geophys. Res. 120, 5273–5289. http://dx.doi.org/10.1002/2015JB011963.

Chester, F.M., 1995. A rheological model for wet crust applied to strike-slip faults. J. Geophys. Res. 100 (B7), 13,033–13,044.

Chester, F.M., Higgs, N.G., 1992. Multimechanism friction constitutive model for ultrafine quartz gouge at hydrothermal conditions. J. Geophys. Res. 97 (B2), 1859–1870.

Coble, C.G., French, M.E., Chester, F.M., Chester, J.S., Kitajima, H., 2014. In situ frictional properties of San Andreas Fault gouge at SAFOD. Geophys. J. Int. 199, 956–967. http://dx.doi.org/10.1093/gji/ggu306.

den Hartog, S.A.M., Peach, C.J., Matthijs de Winter, D.A., Spiers, C.J., Shimamoto, T., 2012. Frictional properties of megathrust fault gouges at low sliding velocities: New data on effects of normal stress and temperature. J. Struct. Geol. 38, 156–171. http://dx.doi.org/10.1016/j.jsg.2011.12.001.

den Hartog, S.A.M., Spiers, C.J., 2013. Influence of subduction zone conditions and gouge composition on frictional slip stability of megathrust faults. Tectonophysics 600, 75–90. http://dx.doi.org/10.1016/j.tecto.2012.11.006.

Eaton, J.P., 1990. The earthquake and its aftershocks from May 2 through September 30, 1983. In: Rymer, M.J., Ellsworth, W.L. (Eds.), The Coalinga, California Earthquake of May 2, 1983. U.S. Geol. Surv. Prof. Pap, 1487, pp. 113–170.

Ekström, G., Stein, R.S., Eaton, J.P., Eberhart-Phillips, D., 1992. Seismicity and geometry of a 110-km-long blind thrust fault. 1. The 1985 Kettleman Hills, California, Earthquake. J. Geophys. Res. 97 (B4), 4843–4864. http://dx.doi.org/10.1029/91JB02925.

Ernst, W.G., 1965. Mineral parageneses in Franciscan metamorphic rocks, Panoche Pass, California. Geol. Soc. Am. Bull. 76, 879–914.

Ernst, W.G., 1970. Tectonic contact between the Franciscan mélange and the Great Valley sequence: crustal expression of a late Mesozoic Benioff zone. J. Geophys. Res. 75, 886–901.

Ernst, W.G., 2011. Accretion of the Franciscan Complex attending Jurassic-Cretaceous geotectonic development of northern and central California. Geol. Soc. Am. Bull. 123 (9/10), 1667–1678.

Ernst, W.G., McLaughlin, R.J., 2012. Mineral parageneses, regional architecture, and tectonic evolution of Franciscan metagraywackes, Cape Mendocino–Garberville–Covelo 30' x 60' Quadrangles, Northwest California. Tectonics 31, TC001. http://dx.doi.org/10.1029/2011TC002987.

Evarts, R.C., Schiffman, P., 1983. Submarine hydrothermal metamorphism of the Del Puerto ophiolite, California. Am. J. Sci. 283, 289–340.

French, M.E., Kitajima, H., Chester, J.S., Chester, F.M., Hirose, T., 2014. Displacement and dynamic weakening processes in smectite-rich gouge from the Central Deforming Zone of the San Andreas Fault. J. Geophys. Res. Solid Earth 119, 1777–1802. http://dx.doi.org/10.1002/2013JB010757.

French, M.E., Chester, J.S., Chester, F.M., 2015. Micromechanisms of creep in clay-rich gouge from the Central Deforming Zone of the San Andreas Fault. J. Geophys. Res. 120, 827–849. http://dx.doi.org/10.1002/2014JB011496.

Hamilton, W., 1969. Mesozoic California and the underflow of Pacific mantle. Geol. Soc. Am. Bull. 80, 2409–2430.

Holdsworth, R.E., Van Diggelen, E.W.E., Spiers, C.J., De Bresser, J.H.P., Walker, R.J., Bowen, L.A., 2011. Fault rocks from the SAFOD core samples: implications for weakening at shallow depths along the San Andreas Fault, California. J. Struct. Geol. 33, 132–144. http://dx.doi.org/10.1016/j.jsg.2010.11.010.

Iiyama, J.T., Roy, R., 1963. Unusually stable saponite in the system Na_2O-MgO-Al_2O_3-SiO_2. Clay Min. Bull. 5, 161–171.

Jennings, C.W., Strand, R.G., Rogers, T.H., 1977. Geologic map of California. Calif. Div. Mines Geol. scale 1, 750,000.

Kristmannsdottir, H., 1979. Alteration of basaltic rocks by hydrothermal activity at 100–300°C. Dev. Sediment. 27, 359–367.

Kuchta, L., Fajnor, V.S., 1988. Optimal conditions for hydrothermal synthesis of saponite. Chem. Pap. 42, 339–345.

Le Pourhiet, L., Saleeby, J., 2013. Lithospheric convective instability could induce creep along part of the San Andreas fault. Geology 41, 999–1002. http://dx.doi.org/10.1130/G34244.1.

Lockner, D.A., Morrow, C., Moore, D., Hickman, S., 2011. Low strength of deep San Andreas Fault gouge from SAFOD core. Nature 472, 82–85. http://dx.doi.org/10.1038/nature09927.

Logan, J.M., Friedman, M., Higgs, N., Dengo, C., Shimamoto, T., 1979. Experimental studies of simulated gouge and their application to studies of natural fault zones. In: Proceedings Conference VIII. Analysis of Actual Fault Zones in Bedrock. U.S. Geol. Surv. Open File Rep. 79-1239, pp. 305–343.

Mackenzie, R.C., 1957. Saponite from Allt Ribhein, Fishkavaig Bay, Skye. Min. Mag. 31, 672–682.

McPhee, D.K., Jachens, R.C., Wentworth, C.M., 2004. Crustal structure across the San Andreas Fault in the SAFOD site from potential field and geologic studies. Geophys. Res. Lett. 31, L12S03. http://dx.doi.org/10.1029/2003GL019363.

Moore, D.E., 2014. Comparative mineral chemistry and textures of SAFOD fault gouge and damage-zone rocks. J. Struct. Geol. 68, 82–96. http://dx.doi.org/10.1016/j.jsg.2014.09.002.

Moore, D.E., Byerlee, J.D., 1991. Comparative geometry of the San Andreas fault, California and laboratory fault zones. Geol. Soc. Am. Bull. 103, 762–774.

Moore, D.E., Lockner, D.A., 2004. Crystallographic controls on the frictional behavior of dry and water-saturated sheet-structure minerals. J. Geophys. Res. 109, B03401. http://dx.doi.org/10.1029/2003JB002582.

Moore, D.E., Lockner, D.A., 2008. Talc friction in the temperature range 25°–400°C: relevance for fault-zone weakening. Tectonophysics 449, 120–132. http://dx.doi.org/10.1016/j.tecto.2007.11.039.

Moore, D.E., Lockner, D.A., 2011. Frictional strengths of talc-serpentine and talc-quartz mixtures. J. Geophys. Res. 116, B01403. http://dx.doi.org/10.1029/2010JB007881.

Moore, D.E., Lockner, D.A., 2013. Chemical controls on fault behavior: weakening of serpentinite sheared against quartz-bearing rocks and its significance for fault creep in the San Andreas system. J. Geophys. Res. 118, 1–13. http://dx.doi.org/10.1002/jgrb.50140.

Moore, D.E., Lockner, D.A., 2015. Correlation of chlorite frictional strength with composition. Eos Trans AGU. 96 (Fall Meeting Supplement). Abstract 21C-2628.

Moore, D.E., Rymer, M.J., 2007. Talc-bearing serpentinite and the creeping section of the San Andreas fault. Nature 448, 795–797. http://dx.doi.org/10.1038/nature06064.

Moore, D.E., Rymer, M.J., 2012. Correlation of clayey gouge in a surface exposure of serpentinite in the San Andreas Fault with gouge from the San Andreas Fault Observatory at Depth. J. Struct. Geol. 38, 51–60. http://dx.doi.org/10.1016/j.jsg.2011.11.014.

Morrow, C.A., Moore, D., Lockner, D.A., 2010. Dependence of frictional strength on compositional variations of Hayward fault rock gouges. In: Knudsen, K., et al. (Eds.), Proceedings Third Conference on Earthquake Hazards in the Eastern San Francisco Bay Area. Calif. Geol. Surv. Spec. Rep. 219, pp. 115–127.

Morrow, C.A., Lockner, D.A., Moore, D.E., Hickman, S., 2014. Deep permeability of the San Andreas Fault from San Andreas Fault Observatory at Depth (SAFOD) core samples. J. Struct. Geol. 64, 99–114. http://dx.doi.org/10.1016/j.jsg.2013.09.009.

Mücke, A., 2003. Fayalite, pyroxene, amphibole, annite and their decay products in mafic clots within Younger Granites of Nigeria: petrography, mineral chemistry, and genetic implications. J. Afr. Earth Sci. 36, 55–71.

Noriega, G.R., Arrowsmith, J.R., Grant, L.B., Young, J.J., 2006. Stream channel offset and late holocene slip rate of the San Andreas Fault at the Van Matre Ranch site, Carrizo Plain, California. Bull. Seismol. Soc. Am. 96, 33–47. http://dx.doi.org/10.1785/0120050094.

Page, B.M., Thompson, G.A., Coleman, R.G., 1998. Cenozoic tectonics of the central and southern Coast Ranges of California. Geol. Soc. Am. Bull. 110 (7), 846–876.

Pollitz, F., 1986. Pliocene change in Pacific plate motion. Nature 320, 731–738. http://dx.doi.org/10.1038/32073890.

Robinson, D., Schmidt, S.Th, Santana de Zamora, A., 2002. Reaction pathways and reaction progress for the smectite-to-chlorite transformation: evidence from hydrothermally altered metabasites. J. Met. Geol. 20, 167–174.

Sanford, R.F., 1982. Growth of ultramafic reaction zones in greenschist to amphibolite facies metamorphism. Am. J. Sci. 282, 543–616.

Schiffman, P., Fridleiffson, G.O., 1991. The smectite-chlorite transition in drillhole NJ-15, Nosjavellir geothermal field, Iceland: BSE and electron microprobe investigations. J. Met. Geol. 9, 679–696.

Schleicher, A.M., Warr, L.N., van der Pluijm, B.A., 2009. On the origin of mixed-layered clay minerals from the San Andreas Fault at 2.5–3 km vertical depth (SAFOD drillhole at Parkfield, California). Contr. Min. Pet. 157, 173–187.

Schleicher, A.M., van der Pluijm, B.A., Warr, L.M., 2012. Chlorite-smectite clay

minerals and fault behavior: New evidence from the San Andreas Fault Observatory at Depth (SAFOD) core. Lithosphere 4 (3), 209–220. http://dx.doi.org/10.1130/L158.1.

Scott, D.R., Lockner, D.A., Byerlee, J.D., Sammis, C.G., 1994. Triaxial testing of Lopez fault gouge at 150 MPa mean effective stress. Pure Appl. Geophys. 142, 749–775.

Soda, Y., Takagi, H., 2010. Sequential deformation from serpentinite mylonite to metasomatic rocks along the Sashu Fault, SW Japan. J. Struct. Geol. 32, 792–802. http://dx.doi.org/10.1016/j.jsg.2010.05.003.

Sone, H., Shimamoto, T., Moore, D.E., 2012. Frictional properties of a metasomatic saponite-rich gouge from a serpentinite-bearing fault zone in the Gokasho-Arashima Tectonic Line, central Japan. J. Struct. Geol. 38, 172–182. http://dx.doi.org/10.1016/j.jsg.2011.09.007.

Stein, R.S., Ekström, G., 1992. Seismicity and geometry of a 110-km-long blind thrust fault 2. Synthesis of the 1982–1985 California earthquake sequence. J. Geophys. Res. 97 (B4), 4865–4883. http://dx.doi.org/10.1029/91JB02847.

Tembe, S., Lockner, D., Wong, T.-F., 2009. Constraints on the stress state of the San Andreas Fault with analysis based on core and cuttings from San Andreas Fault Observatory at Depth (SAFOD) drilling phases 1 and 2. J. Geophys. Res. 114, B11401. http://dx.doi.org/10.1029/2008JB005883.

Tembe, S., Lockner, D.A., Wong, T.-F., 2010. Effect of clay content and mineralogy on frictional sliding behavior of simulated gouges: Binary and ternary mixtures of quartz, illite, and montmorillonite. J. Geophys. Res. 115, B03416. http://dx.doi.org/10.1029/2009JB006383.

Titus, S.J., DeMets, C., Tikoff, B., 2006. Thirty-five year creep rates for the creeping segment of the San Andreas Fault and the effects of the 2004 Parkfield earthquake: constraints from alignment arrays, continuous global positioning system, and creepmeters. Bull. Seismol. Soc. Am. 96 (4B), 5250–5268.

Titus, S.J., Dyson, M., DeMets, C., Tikoff, B., Rolandone, F., Bürgmann, R., 2011. Geologic versus geodetic deformation adjacent to the San Andreas fault, central California. Geol. Soc. Am. Bull. 123 (5/6), 794–820. http://dx.doi.org/10.1130/B301501.

Whitney, D.L., Evans, B.W., 2010. Abbreviations for names of rock-forming minerals. Am. Min. 95, 185–187.

Wilson, M.J., Bain, D.C., 1970. The clay mineralogy of the Scottish Dalradian metalimestones. Contr. Min. Pet. 26, 285–295.

Zoback, M., Hickman, S., Ellsworth, W., 2010. Scientific drilling into the San Andreas fault zone. Eos Trans. AGU 91 (22), 197–199.

Zoback, M., Hickman, S., Ellsworth, W., 2011. Scientific drilling into the San Andreas Fault Zone — An overview of SAFOD's first five years. Sci. Drill. 11, 14–28.